Ultra-Low Frequency DC-DC Converters Using Switched Batteries

Emeric Perez, Carlos Augusto Berlitz, Yasser Moursy, Bruno Allard, Sami Oukassi, Gael Pillonnet

Ultra-Low Frequency DC-DC Converters Using Switched Batteries

Emeric Perez
Univ. Grenoble Alpes, CEA, LETI
F-38000 Grenoble, France
emeric.perez@cea.fr

Carlos Augusto Berlitz
Univ. Grenoble Alpes, CEA, LETI
F-38000 Grenoble, France

Yasser Moursy
Univ. Grenoble Alpes, CEA, LETI
F-38000 Grenoble, France

Bruno Allard
Univ Lyon, INSA Lyon, CNRS, Ampere
F-69621 Villeurbanne, France

Sami Oukassi
Univ. Grenoble Alpes, CEA, LETI
F-38000 Grenoble, France

Gaël Pillonnet
Univ. Grenoble Alpes, CEA, LETI
F-38000 Grenoble, France
gael.pillonnet@cea.fr

***Abstract*—To address ultra-low frequency DC-DC converters, we explore the concept of the switched battery converter. It is mainly derived from the switched capacitor converter topology replacing the flying capacitors by flying batteries. The best-in-class energy density of batteries compared to inductors and capacitors reduces drastically the operating frequency at low output power delivery while maintaining low output ripple. An experimental evaluation using mm^3-scale off-the-shelf NiMH battery is described in this paper to present a first proof-of-concept of *switched-battery* converter. The characterized 2:1 DC-DC converter achieves 25mW at 1.2V output voltage in 74mm^3 battery operating as low as 0.1 Hz operating frequency while maintaining less than 15% output voltage ripple without output filtering.**

***Index Terms*—Switching converter, battery, switched capacitor converter, DC-DC converter.**

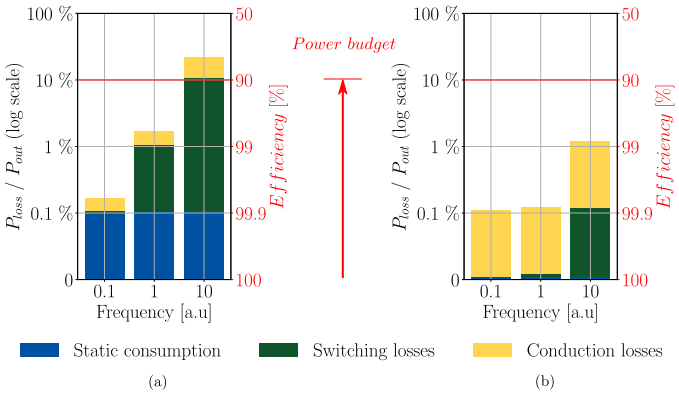

Fig. 1: Losses in a converter against frequency [schematic example]: (a) Low power case (b) High power case

I. Introduction

In the context of fully integrated voltage regulators (FIVR), the footprint of DC-DC converters is mainly limited by the passive components (capacitors, inductors). The switched capacitors converters (SCC) have been considered as good candidates thanks to high power density and integrability in CMOS technology compared to inductors below the cm^3 scale [1] - [2]. The SCC output impedance is inversely proportional to the product of the capacitor value C_{fly} and the operating frequency f_{sw} [3]. Hence, increasing the operating frequency by 10× reduces more or less the footprint of the passive component with a similar factor. However, the switching losses are increased by 10× thus reducing the power efficiency. At low power - e.g. mW scale and below - as illustrated in Fig. 1 the switching losses limit the achievable operating frequency if maintaining an efficiency larger than 90%. As the operating frequency is limited, capacitors with higher capacitance density are an alternative to increase the power density (W/mm^3) [4]-[5]. Nevertheless, the increase in the capacitance density is limited up to few 200 nF/mm^2 [6] (deep-trench capacitors), failing to maintain non-negligible switching loss at low power. Alternatively to capacitor and inductor, a third energy storage option is explored in this paper: the battery.

Batteries exhibit more than three order of magnitude higher energy density compared to traditional passives thanks to a volumetric based energy storage of ions. Solid-state batteries prior art proved the feasibility of high energy density even at mm^3-scale µ-batteries [9] and open the possibility of smart integration in a single chip. Based on this excellent energy property, we propose to replace capacitors by batteries in a new converter concept called switched battery converters (SBC). Employing batteries allow to work at ultra-low operating frequencies (Hz range) and maintain low output ripple, thus reduces the switching losses at low output power delivery. High efficiency at low power is essential for IoT applications, especially to power always-on IPs (Integrated Processors) such oscillators or wake-up radio. Nevertheless, batteries suffer from limited power capability and life cycle if large depth of discharge is experienced. Maximum power achievable for the battery comes from the current limit. This paper explores the capability of mm^3-scale NiMH battery as a candidate for DC-DC power conversion at low power (in mW range). Firstly the key enabler of batteries compared to passives is emphasized, then we show the battery response imposed by the DC-

TABLE I: OFF-THE-SHELF DEVICES SAMPLE WITH MM^3 VOLUME

Passive	Metric	Energy density $[J.mm^{-3}]$	Power density $[W.mm^{-3}]$	Power density $[\mu W.mm^{-3}]$	Voltage/current rating	ESR $[\Omega]$	Volume $[mm^3]$
	Frequency	-	@ SRF/10	@ 1 Hz			
Battery (V6HR)		3.6×10^{-1}	N.A	360	0.018 A	6	74
Capacitor [7]		5×10^{-3}	2	50	6.3 Vdc	15×10^{-3}	60
Inductor [8]		7×10^{-8}	0.01	0.07	0.145 A	2.9	69

DC converter mission profile. The battery is finally included in an step-down SBC to give some experimental results on achievable performances. A comparison to prior art is given to provide figures of merit. Furthermore, a discussion section underlines both passives inherent limitations and batteries possible optimization for SBC usage.

II. BATTERY: AN ALTERNATIVE?

To understand the fundamental differences between batteries and traditional passives, we have to look at the mechanisms of energy storage. Traditional passives rely on storage of charges on a surface (capacitor) or magnetic field in a volume (inductor), while battery stores energy inside a volumetric crystalline structure. Besides electrostatic and electromagnetic processes are fast compared to chemical reactions involved in batteries thus providing higher power density to capacitors and inductors.

In regards to [3] the power and energy density strongly depend on the passive component size. Tab. I compares three selected components wih similar volume, i.e. mm^3-scale, corresponding to typical coin battery size. They share low voltage/current ratings - lower than 6.3V and 0.145A to compare similar devices. Battery energy density is 1,000× higher compared to their counterparts. The maximum battery power density is 10,000× lower than for the one of capacitor and inductor because the amount of power delivered by the battery is independent from the self-resonance frequency (SRF) but limited by the maximal allowed current. If high efficiency at low power level is targeted, the operating frequency is limited to few Hz as mentioned in [10] and shown in the schematic of Fig. 1. Power density of the battery at 1 Hz is hence similar to the one of capacitor and significantly higher than the one of inductor.

III. BATTERY µ-CYCLE

As illustrated in Tab. I batteries are competitive in the Hertz range compared to other passives. SBC operation mode requires the battery to experience radically different usage profile in comparison with large State of Charge (SoC) utilization in hours scale. SBC operation creates a new usage profile for batteries which has not been explored yet in prior art. A battery under test (BUT) has been then introduced to depict their innovative ability to be cycled in μ-Coulomb-scale to milli-Coulomb-scale at second time scale for mimicking SBC operation mode. Such usage profile involves only a small-displacement Q_E - much less than a percent of battery capacity - around a bias point as illustrated in (V,Q) characteristic in Fig. 2(b). This bias point Q_{DC} is chosen at 50% State of Charge (SoC) point as the battery resistance is here minimal. In the following, the SBC mission profile of the battery is called *μ-cycle*. Aiming to explore off-the-shelf battery, we chose a 74 mm^3 NiMH battery model (V6HR) of 1.2 V nominal voltage (V_{bat}) within the power range batteries. The nominal capacity of our BUT is 6 mAh and the manufacturer DC current limit I_{lim} is fixed at 3C (C-rate, equivalent to 18 mA). Battery DC resistance (R_{int}) is given by the manufacturer to be 6 Ω. BUT has been then chosen to meet the milliwatt power delivery initial requirement.

Considering the SBC power density to be inherently limited by the impedance of the BUT, a small-signal impedance Z_{bat} against frequency has been acquired experimentally with Electrochemical Impedance Spectroscopy (EIS) around the 50% SoC point. As shown in Fig. 2(a) the real part of the impedance is dominant below the kHz and roughly equal to the battery DC resistance. Impedance magnitude varies around the value of 6 Ω with only a factor of 3 over four decades of frequency. The battery can be used up to ten of kHz, with a resonance frequency around the hundred of kHz. As a first approach, the maximum battery output power level P_{max} is limited to ${V_{bat}}^2/4Z_{bat}$ which gives 60 mW. Nevertheless several electrochemical limitations are not assessed with small-signal analysis as it implies currents far lower than 1C order of magnitude. A quasi-static current limit (I_{lim}) is indeed fixed by the electrochemical stability potential window of the battery electrolyte limiting the maximal output power level [11] [12] in full charging/discharging conditions. In practice the achievable battery quasi-static power is given by $V_{bat} \times I_{lim}$, here 22 mW which is lower than the calculated P_{max}. BUT power indicated in Tab. I is a little bit higher as it corresponds to tested BUT power under μ-cycle.

The battery impedance also depends on the current level because of limited rate for ion transfer under large operating currents, i.e. above 1C [13]. Consequently the small-signal analysis has to be complemented with a *large-signal* characterization of the BUT.

To assess large-signal characterisation, a rectangular current wave of amplitude $I_{bat,in}$ (mA range) and frequency f_{sw} (Hz range) with zero mean value has been applied to our

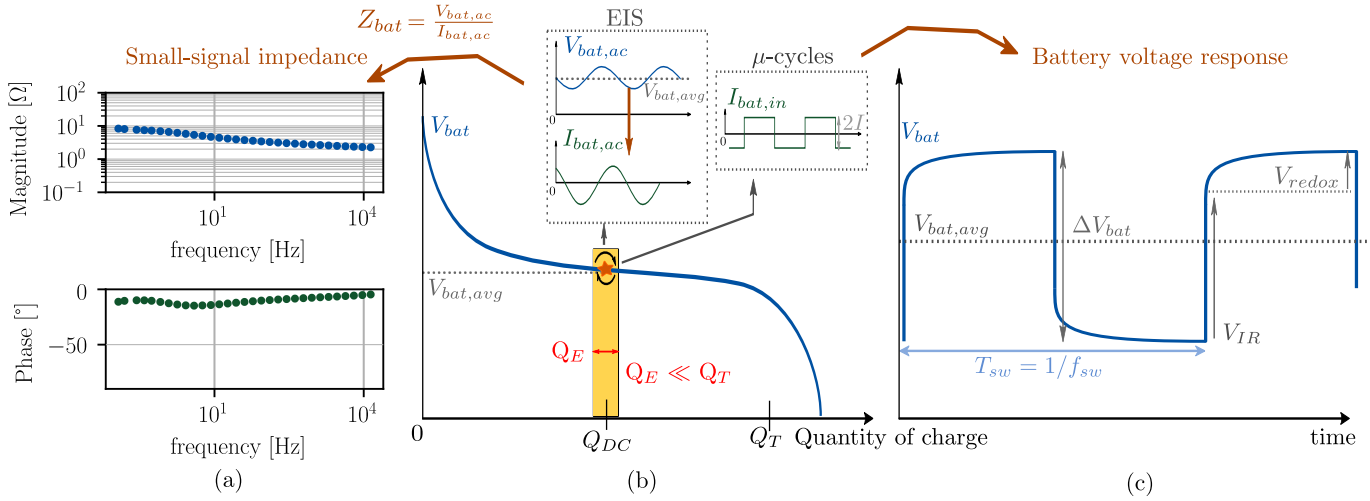

Fig. 2: (a) Experimental small-signal impedance of the battery (b) (V,Q) characteristic of the battery (c) Schematic battery voltage response to microcyles

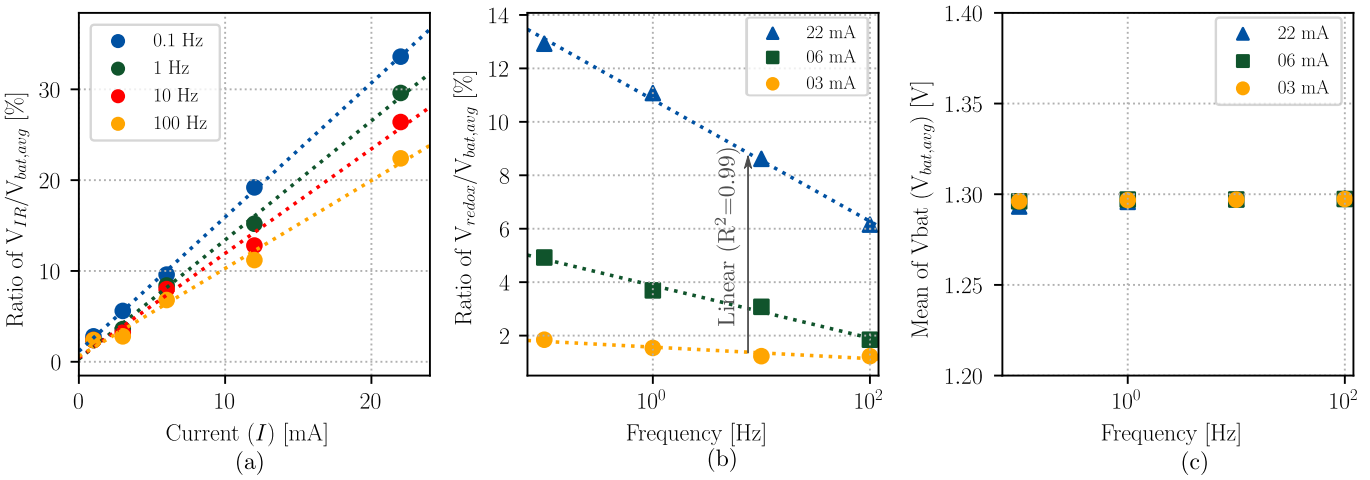

Fig. 3: Experimental curves : (a) IR drop voltage to a current (b) Ionic voltage component to a frequency (c) Mean voltage value of the battery (relaxed)

BUT to reproduce SBC μ-cycle operation. Fig. 2(b) and Fig. 2(c) respectively details SBC μ-cycle operation and the resulting voltage response acquisition. Two major voltage components - representing the large signal battery behavior - in BUT response has been identified in Fig. 2(c): i) IR drop V_{IR} due to the internal resistance ii) redox voltage V_{redox} related to redox reactions occuring upon μ-cycling. As expected, the IR drop is linearly correlated to current as shown in Fig. 3(a). The resistance extracted from the slope in Fig. 3(a) is $R_{\mu c}$ and gives 7Ω +/- 15% over three frequency decades. $R_{\mu c}$ is slightly different from R_{int} and previously obtained small-signal impedance highlighting the interest of large-signal characterization. A small frequency dependance is observed in IR drop as it has been previously observed in small-signal analysis in Fig. 2(a). Redox voltage follows a logarithmic frequency law which denotes a superposition of chemical mechanisms detailed in [13]: i) a ion diffusion phenomenon, chemically defined as function of the square root of time ; ii) a charge transfer process, corresponding to a small-displacement on the (V,Q) characteristic. Moreover, it appears that redox voltage evolves more or less linearly with respect to current (R^2=0.99, @ 10 Hz) as shown with gray arrow in Fig. 3(b). To summarize, ionic voltage decreases with frequency while both redox voltage and IR drop increases with current.

We observed that the battery average voltage ($V_{bat,avg}$) is close to the open-circuit relaxed potential (OCRV) under rectangular current wave input, in steady-state conditions. This value is independent from the rectangular current level as well as the frequency as shown in Fig. 3(c) what constitutes a new result. Moreover, $V_{bat,avg}$ is stable over 10^7 μ-cycles, while operating at the battery current limit under rectangular current wave. It indicates an extended cycle life of batteries under μ-cycles as compared to usual cycle life of NiMH batteries (10^3 cycles rated by the manufacturer) in accordance to [14].

IV. Switched Battery Converters

The BUT is incorporated in an widely adopted DC-DC power stage called SBC inspired from SCC. Our

implementation is a 2:1 step-down converter as shown in Fig. 4a. More optimal power stage could be be proposed but for clarity purposes, we have adopted the most classical topology for easier comparison with capacitive-based converterters. In open-circuit condition the output voltage is half of the input voltage. The SBC is composed of four switches (0.25 Ω on-state resistance) and a single flying battery. One cycle consists of two equal duration phases. During the first phase ϕ_1 the battery is connected in series with the input voltage source (V_{in}) and the output voltage (V_{out}). The battery receives a charge Q_1 equal to $I_{out}t_{\phi_1}$. During a second phase ϕ_2 the battery is partially discharged through the load. The battery releases Q_2 charges ($I_{out}t_{\phi_2}$).

In SBC, the amount of charge transfer into the battery Q_E is far from Q_{DC}. The battery experiences hence very small SoC variation (<1%). If perfect charge balancing is assumed the battery returns to its initial state of charge Q_{DC}. If perfect charge balancing is not respected, a battery monitoring can be implemented. Thanks to expected low SoC drift ($Q_E/Q_{DC} \ll 1$) monitoring would be activated intermittently.

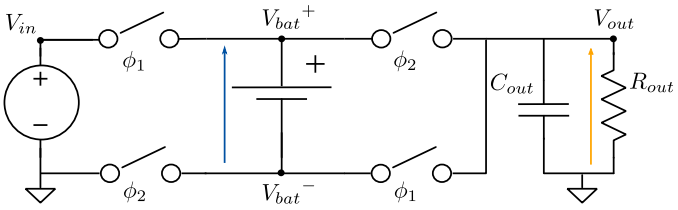

(a)

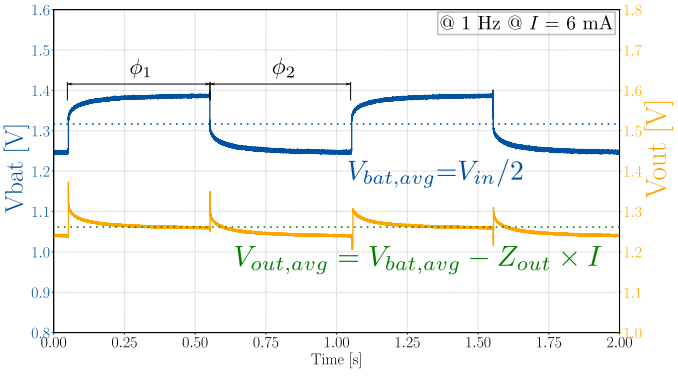

(b)

Fig. 4: (a) Electrical schematic of a 2:1 SBC and (b) Experimental voltage curves of battery and output in a SBC (without output capacitor) in steady-state

Battery and output voltage experimental waveforms are given in Fig. 4b when the output current and operating frequency are 6 mA and 1Hz, respectively. The battery voltage follows the same shape as introduced in Fig. 2(c).

Aforementioned, the average battery voltage $V_{bat,avg}$ is independent from I_{out} but its value is dependent on the input voltage. Under long-time scale - e.g much greater than hour, to let chemical species concentrations reach their new equilibrium point - $V_{bat,avg}$ will tend to the value of $V_{in}/2$ denoted $V_{bat,st}$. It demonstrates that battery in SBC doesn't behave anymore as a constant voltage source but as an adaptative voltage source to the input. Careful design considerations must be hence taken to ensure that the value of $V_{in}/2$ doesn't exceed the maximum battery voltage rating.

The average output voltage $V_{out,avg}$ of SBC can be expressed as (1).

$$|V_{out,avg}| = |\frac{R_{load}}{R_{load} + Z_{out}}|\frac{V_{in}}{2} \quad (1)$$

Where R_{load} is the load resistance and Z_{out} the SBC output impedance.

The output impedance is derived from the series combination of on-switch resistance and $R_{\mu c}$ assuming hence negligible charge-sharing losses compared to SCC.

The output voltage ripple shown in Fig. 4b is due to the redox voltage component of the battery as defined in Section III. If input voltage level changes abruptly an extra-ripple component equal to $V_{in} - 2V_{bat,avg}$ appears on the output while $V_{bat,avg}$ is different from $V_{bat,st}$. Hence, battery high energy density becomes a penalty in the case of fast SBC dynamic responses.

Conduction effciency η_c (e.g without switch drive loss) of SBC is depicted in Fig. 5(a) and can be roughly estimated using :

$$\eta_c = \frac{R_{load}}{R_{load} + \Re(Z_{out})} \quad (2)$$

SBC features 14.3 mW @ 90% conduction efficiency *at only* 0.1 Hz. SBC output power varies slightly over three decades of operating frequency (0.1 Hz to 10 Hz) showing frequency independance. A SCC featuring a passive of mm^3 scale (respectively $74mm^3$ and $59mm^3$ for SBC and SCC) operates at 10× higher operating frequency (100 Hz) compared to SBC. SCC fails to provide the same output power level as SBC below 100 Hz showing large contribution of charge sharing losses at such low frequency. High induced charge sharing losses limit drastically the power capability of capacitors components as introduced in Section II.

Fig. 5(b) shows the depth of discharge (DoD) against output power. The DoD is defined by Q_E/Q_T where Q_T is the nominal capacity. In SBC the DoD is lower than 10^4 ppm at maximal output power level and can be linearly scaled down with frequency. This low DoD allows extended battery life-cycle as reported in [14], enabling battery life-time to be compatible with continous switching operation.

Fig. 5(c) explores the relative output voltage ripple ($\Delta V_{out}/V_{out,avg}$) against output power. V_{in} in SBC has

been set to twice the average battery voltage to minimize the ripple (under short-time scale). Even at 0.1 Hz and without any output decoupling capacitors the ripple is limited to a moderate 15% @ 25mW. The maximal ripple is 4× higher using SCC operating at 1,000× higher frequency.

A second battery used in SBC as an output filter seems to be not beneficial as the battery sees the switching edges and responds to it with limited dynamics i.e. voltage peaks. Nevertheless, a decoupling capacitor can be added to the output to further reduce the moderate output voltage ripple without significant extra area cost.

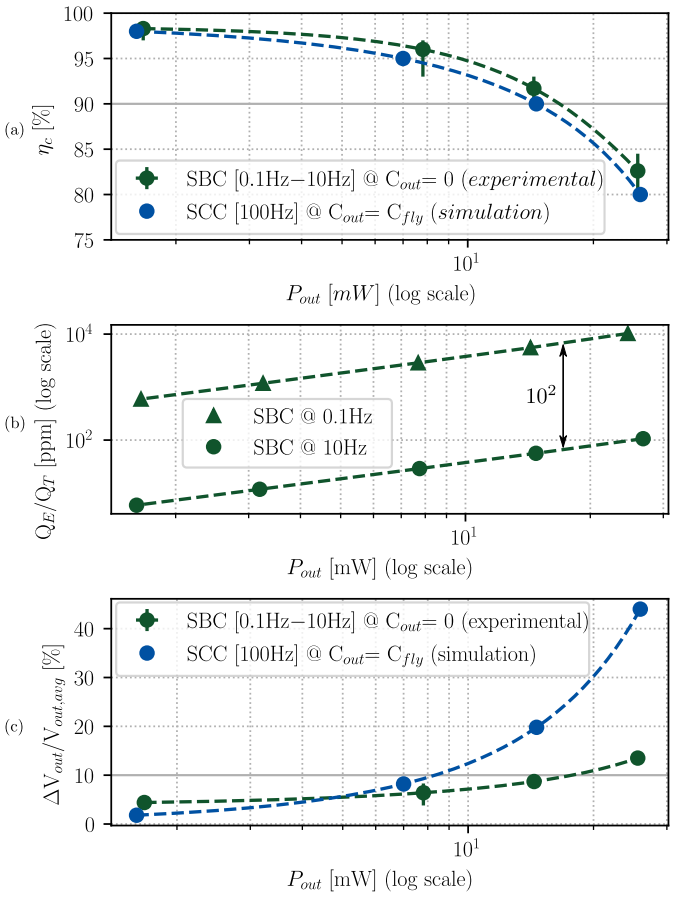

Fig. 5: (a) Conduction efficiency (without switch drive loss) against P_{out} (b) Relative charge storage utilization (c) Relative output voltage ripple

V. Performance comparison

The proposed SBC is compared to existing DC-DC converters providing the same output power level. Fig. 6(a) illustrates converter energy density versus converter power density both estimated from litterature data. A declination of the proposed SBC has been achieved with another battery model called V150H (NiMH). V150H battery features one order higher in size scale compared to V6HR battery. Converter energy density is defined as the energy stored in the converter considering the passive or battery volume. For SCC the flying silicon capacitor area is estimated from reference data and we assumed 1 mm of die thickness. For inductive converters the off-chip inductor volume is estimated from off-the-shelf CMOS inductors.

In Fig. 6(a) the converter power density is the maximum output power density at peak efficiency. The SBC energy density is far higher than prior art but enhances a lower power capability. These considerations confirm the fundamental differences between batteries and passives introduced in Section II. Even if power density is one keypoint for converter design, energy density is also a key enabler to provide low output ripple at low operating frequency.

Fig. 6(b) illustrates this statement by introducing a Figure-of-Merit based on the passive energy utilization rate against the inverse of the maximal operating frequency by using $M_F = 1/f_{sw,max}$. To assess the ability of a converter to achieve low output ripple without output filtering, M_E is introduced and defined by:

$$1/M_E = \frac{\Delta E_{trans}}{E_{store}} \tag{3}$$

Where ΔE_{trans} is the energy transfered to the output during a converter period, E_{store} is the energy continuously stored in the converter. ΔE_{trans} is calculated using the output power at peak efficiency considering maximal reported operating frequency ($f_{sw,max}$). E_{store} is estimated from an average bias current or bias voltage of the passives.

As mentionned in the paper motivation, low operating frequency leverages efficiency at low power. Higher M_F shows better ability to fulfill this target.

Even if SBC operates at operating frequency four order of magnitude lower, SBC features high M_E meaning ability to provide low output ripple without output filtering. To counteract the low M_E (high passive energy utilization) in reported litterature an output capacitor or interleaved scheme may be added to maintain acceptable output ripple. This strategy leads to additional passive components thus reducing the overall power density.

VI. Discussion

Passive energy density is inherently limited because of technological feasibility on the dielectric and magnetic materials. According to [4] the product of the dielectric permitivity ε_r and the maximum electric field in CMOS capacitors dielectric (CM) is empirically limited to approximatelly 400 $V^2.cm^{-2}$. Based on this value, maximal capacitor energy density is then bounded by 10^{-2} J/mm^3 using the following formulae : $(1/2)\varepsilon_0 CM$. Magnetic energy density is defined as the product of the magnetic flux density B and the magnetic field density H. Currently [15] gives a magnetic cores maximal energy density to be equal to 59 MGoe (Mega Gauss Oersteds) at room temperature

(Nd-Fe-B material). Taking half of this product gives the inductor energy density limit which is roughly equal to 10^{-4} J/mm^{-3}. These results are shown in Fig. 6(a) and they are in accordance with [16].

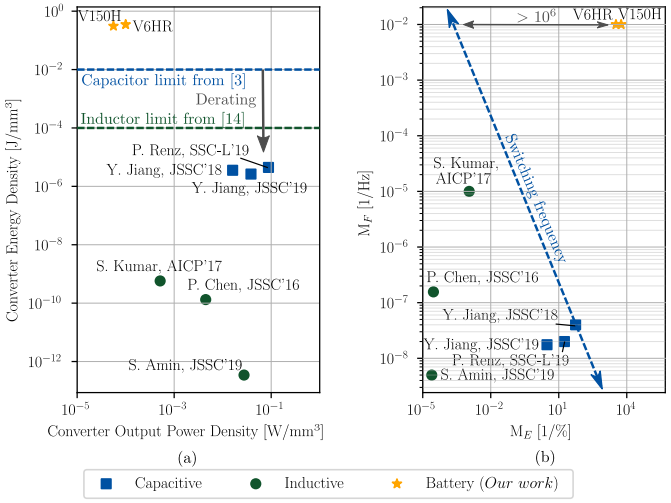

Fig. 6: Converter energy versus power (a) FoM graph (b)

Passives devices in general cannot reach the level of V6HR and V150H selected batteries as shown in Fig. 6(a). Derating in converter energy density is observed in Fig. 6(a) as a consequence of design margins, packaging size, manufacturing constraints. Blue dotted arrow in Fig. 6(b) denotes the displacement of one litterature reference if operating frequency were tuned ($M_E \times M_F = constant$). Considering the same M_E ratio, batteries would feature always either a lower size or lower operating frequency compared to other passive devices.

Solid-state batteries may be considered to envisage a fully integrated SBC version. Using solid-state batteries manufacturing techniques open the way to a fine-grain co-optimization of battery power and energy density. As the energy density gap between batteries and other passive devices is high, a slight decrease in battery energy density to gain power delivery capability by co-optimization is tolerable.

Operating at relatively low-power levels i.e. inside the battery safe operating current limit prevents thermal management issues. Battery internal resistance power losses can be then dissipated on the relatively large considered battery surface (0.7 mW/mm^2).

Battery ageing concerns under SBC operation hasn't been deeply investigated in this study due to timing constraints. Nervertheless, [17] suggests that spending time within high battery charging / discharging states (respectively high and low SoC) is a key contributor to battery ageing. Hence, using a 50% SoC biasing point seems to be a preventive action to counteract battery ageing. Three months of "intensive" experiments - e.g. 500 hours of experiment with accumulated 1 billion μ-cycles - using a single battery sample showed no noticeable battery voltage drifts nor internal resistance shifts suggesting not accelerated battery ageing under SBC operation mode.

V6HR and V150H batteries are NiMH based batteries but Li-ion batteries have been also successfully tested upon μ-cycle operation in a SBC. Consequently, SBC is not limited to NiMH technology but further investigation has to be made to explore the advantages and disdavantages of each battery technology for SBC applications.

This paper firstly introduced the SBC concept in open-loop but future works are required to explore close-loop structure to regulate the output voltage. SCC usually uses frequency-based control which is not envisageable for SBC as their output impedance is almost frequency independent at first order. A two stages regulation scheme could be adopted: a coarse-grain voltage regulation is insured by SBC while a LDO [18] can be placed at the SBC output to fine-grain regulate output voltage considering low differential voltage and hence high LDO efficiency.

VII. Conclusion

The presented work deals with an innovative architecture of μ-power converter based on a battery (SBC). Thanks to best-in-class energy density, batteries allow ultra-low operating frequency and low output ripple. A first presented prototype achieves 340μW/mm^3 with 25 mW maximal tested power while maintaining 84% conduction efficiency using off-the-shelf battery (V6HR). The output voltage ripple is limited to 1.2% at 1/10 of maximal power capability even if the operating frequency is reduced to 0.1 Hz.

References

[1] C. Ó. Mathúna, N. Wang, S. Kulkarni, and S. Roy, "Review of Integrated Magnetics for Power Supply on Chip (PwrSoC)," *IEEE Transactions on Power Electronics*, vol. 27, no. 11, pp. 4799–4816, Nov. 2012.

[2] R. May, "Analysis of soft charging switched capacitor power converters," Ph.D. dissertation, University of Illinois, Jan. 2014. [Online]. Available: http://hdl.handle.net/2142/46665

[3] M. D. Seeman, V. W. Ng, H.-P. Le, M. John, E. Alon, and S. R. Sanders, "A comparative analysis of Switched-Capacitor and inductor-based DC-DC conversion technologies," in *2010 IEEE 12th Workshop on Control and Modeling for Power Electronics (COMPEL)*, Jun. 2010, pp. 1–7, iSSN: 1093-5142.

[4] H. Johari and F. Ayazi, "High-Density Embedded Deep Trench Capacitors in Silicon With Enhanced Breakdown Voltage," *IEEE Transactions on Components and Packaging Technologies*, vol. 32, no. 4, pp. 808–815, Dec. 2009.

[5] T. M. Andersen, F. Krismer, J. W. Kolar, T. Toifl, C. Menolfi, L. Kull, T. Morf, M. Kossel, M. Brändli, and P. A. Francese, "A 10 W On-Chip Switched Capacitor Voltage Regulator With Feedforward Regulation Capability for Granular Microprocessor Power Delivery," *IEEE Transactions on Power Electronics*, vol. 32, no. 1, pp. 378–393, Jan. 2017.

[6] L. Chang, R. K. Montoye, B. L. Ji, A. J. Weger, K. G. Stawiasz, and R. H. Dennard, "A fully-integrated switched-capacitor 2:1 voltage converter with regulation capability and 90% efficiency at 2.3A/mm2," in *2010 Symposium on VLSI Circuits*, Jun. 2010, pp. 55–56, iSSN: 2158-5636.

[7] L. Murata Manufacturing Co., "ECASD40J157M015K00." [Online]. Available: https://www.murata.com/en-eu/products/productdetail?partno=ECASD40J157M015K00

[8] ——, "LQH44NN471K03." [Online]. Available: https://www.murata.com/en-eu/products/productdetail?partno=LQH44NN471K03%23

[9] S. Oukassi, A. Bazin, C. Secouard, I. Chevalier, S. Poncet, S. Poulet, J.-M. Boissel, F. Geffraye, J. Brun, and R. Salot, "Millimeter scale thin film batteries for integrated high energy density storage," in *2019 IEEE International Electron Devices Meeting (IEDM)*, Dec. 2019, pp. 26.1.1–26.1.4.

[10] A. Paidimarri and A. P. Chandrakasan, "10.8 A Buck converter with 240pW quiescent power, 92% peak efficiency and a 2×106 dynamic range," in *2017 IEEE International Solid-State Circuits Conference (ISSCC)*, Feb. 2017, pp. 192–193, iSSN: 2376-8606.

[11] A. Méry, S. Rousselot, D. Lepage, and M. Dollé, "A Critical Review for an Accurate Electrochemical Stability Window Measurement of Solid Polymer and Composite Electrolytes," *Materials*, vol. 14, no. 14, p. 3840, Jan. 2021.

[12] S. Lee and J. Kim, "Power Capability Analysis of Lithium Battery and Supercapacitor by Pulse Duration," *Electronics*, vol. 8, no. 12, p. 1395, Dec. 2019.

[13] A. Barai, K. Uddin, W. D. Widanage, A. McGordon, and P. Jennings, "A study of the influence of measurement timescale on internal resistance characterisation methodologies for lithium-ion cells," *Sci Rep*, vol. 8, no. 1, p. 21, Jan. 2018.

[14] J. W. Evans, B. Kim, S. Ono, A. C. Arias, and P. K. Wright, "Multicycle Testing of Commercial Coin Cells for Buffering of Harvested Energy for the IoT," *IEEE Internet of Things Journal*, vol. 8, no. 12, pp. 10 047–10 051, Jun. 2021.

[15] S. Sugimoto, "Current status and recent topics of rare-earth permanent magnets," *J. Phys. D: Appl. Phys.*, vol. 44, no. 6, p. 064001, Feb. 2011.

[16] P. A. Kyaw, A. L. F. Stein, and C. R. Sullivan, "Fundamental Examination of Multiple Potential Passive Component Technologies for Future Power Electronics," *IEEE Transactions on Power Electronics*, vol. 33, no. 12, pp. 10 708–10 722, Dec. 2018.

[17] N. Grillon, É. Bouyssou, S. Jacques, and G. Gautier, "Cycle life and statistical predictive reliability model for all-solid-state thin film microbatteries," *Microelectronics Reliability*, vol. 93, pp. 102–108, Feb. 2019.

[18] A. Quelen, G. M. Marega, S. Bouquet, I. Miro-Panades, and G. Pillonnet, "LDO-Assisted Voltage Selector Over 0.5-to-1V VDD Range for Fine Grained DVS in FDSOI 28nm with 200ns/V Controlled Transition," in *ESSCIRC 2018 - IEEE 44th European Solid State Circuits Conference (ESSCIRC)*, Sep. 2018, pp. 202–205.